Радиофизика и радиоастрономия, 2006, т. 11, №3, с. 221-241

Optical and Radio Frequency Diagnostics of the Ionosphere over the Sura Facility: Review of Results

L. M. Kagan, M. J. Nicolls[1], M. C. Kelley[1], V. L. Frolov[2], V. V. Belikovich[2], N. V. Bakhmet'eva[2], G. P. Komrakov[2], D. I. Nedzvetski[2], V. P. Uryadov[2], Yu. M. Yampolski[3], V. G. Galushko[3], A. V. Koloskov[3], A. V. Zalizovski[3], S. B. Kasheev[3], N. F. Blagoveshenskaya[4], V. A. Kornienko[4], T. D. Borisova[4], A. V. Gurevich[5], G. G. Vertogradov[6], V. G. Vertogradov[6], T. S. Trondsen[7], and E. Donovan[7]

University of Western Ontario,
1151 Richmond Street, Suite 2, London, Ontario, Canada

[1]*Cornell University,*
410 Thurston Ave, Ithaca NY 14850-2488, U.S.A.

[2]*Radiophysical Research Institute,*
Bol'shaja Pecherskaja, 25, Nizhniy Novgorod, 603950, Russia

[3]*Institute of Radio Astronomy, NAS Ukraine,*
4, Krasnoznamennaya st., Kharkov, 61002, Ukraine
E-mail: yampol@rian.kharkov.ua

[4]*Arctic and Antarctic Research Institute,*
Beringa, 38, St. Petersburg, 199226, Russia

[5]*Lebedev's Institute of Physics,*
Leninkiy Prospect, 53, GSP-1, Moscow, 119991, Russia

[6]*Rostov-on-Don State University,*
Prospect Stachki, 200/1, Rostov-on-Don, Russia

[7]*University of Calgary,*
2500 University Drive NW Calgary, Alberta, Canada T2N 1N4

Received July 17, 2006

We give an overview of the design and results of the optical-backscatter-heating campaign which we conducted at the Sura facility near Nizhniy Novgorod, Russia on August 10-20, 2004. This campaign was the first to combine optical observations with simultaneous plasma diagnostics by the method of artificial periodic irregularities and with multi-position backscatter measurements and is an example of the clustering of instruments for the purpose of enhancing research results. Some of the results of the campaign have been published in a special issue of Radiophysics and Quantum Electronics and in Physical Review Letters and will only be summarized here. New results include offset of the optical emissions by $1 \div 2°$ from magnetic zenith; broadening of the backscatter spectrum for heating at the fourth harmonic of the electron gyro frequency; observation of self-scattered signals at the second harmonic of the heater fre-

quency; first observations of vector plasma drift/electric field measurements using field-aligned irregularities as tracers; verifying the refractive index mechanism for the Doppler shift of self-scattered signals and first observations of synchronized variations in self-scattered and backscattered signals. The electric field observations confirm that the ionosphere over a mid-latitude site such as SURA can be affected by high latitude processes.

1. Introduction

The optical-backscatter-heating campaign took place at the Sura facility (the geographical coordinates are 56.13° N, 46.10° E, the magnetic dip angle is 71°, the declination angle 10°) on August 10-20, 2004. The goal of the campaign was to accomplish, as completely as possible, 3D diagnostics of natural and induced processes in the ionosphere and neutral atmosphere using multi-instrument remote sensing of the HF-illuminated volume. This campaign was the first to combine optical observations with simultaneous plasma diagnostics by the method of artificial periodic irregularities and with multi-position backscatter measurements. We complemented our diagnostics by making use of the recently discovered self-scattering effect [1] based on the distant receiving of the fundamental and second harmonics of the transmitted signal (including an approximately 16,000-km long-distance reception along the path Sura – Antarctica) [2]. We also recorded geomagnetic field variations in the immediate proximity of the transmitter site to compare dynamic effects in the heated volume with geomagnetic field data.

The first part of the experiments (August 10-15, 2004) was devoted to studying low-altitude ionospheric processes by inducing sporadic E-associated airglow [3-4] with simultaneous diagnostics by the method of artificial periodic irregularities [5-6]. In the second part of the observations (August 16-20, 2004) we planned to study the F-region processes. Multi-position backscatter observations of the heated volume were carried out throughout both parts of the campaign. The first part of the campaign includes the special consideration for carefully choosing the time of the experiment which has an optimal combination of maximum occurrence of sporadic ionization, maximum dark time for optical observations, and a high enough F-region critical frequency to reflect the transmitted radiowaves. Measurements of this type were expected to allow reconstruction of sporadic ionization structure and the 3D neutral wind velocity vector in the E-region proposed in [4-5] and the 3D drift velocity and estimates of electric and magnetic fields in the F-region [7-9].

The advantage of Sura over other operating powerful radiowave facilities which are all located at high latitudes (the only other midlatitude heating facility in Arecibo, Puerto Rico, was destroyed by a hurricane in 1999) is that as a midlatitude facility it lacks a great number of sources of energy present at high latitudes. Sura's disadvantage is the lack of its own optical instrumentation, which prevents optical observations on a routine basis.

Some of the results of the campaign have been already published [10] and some are in press in the special issue of Radiophysics and Quantum Electronics devoted to the VI URSI Suzdal Symposium in October 2004, which held a special workshop on our Sura campaign in August 2004 [11]. In this paper we give an overview of all results from our campaign with only a brief description of the previously published effects.

The paper is organized as follows. We describe all instruments and techniques in Section 2. We give short introductions to previous work in each of Sections 3-7. We start with a brief overview of the results obtained with the use of the artificial periodic irregularities (API) technique in Section 3 (more details can be found in [10-11]). In Section 4 we report the main results from the optical observations, including a brief description of our discovery of the hydroxyl red artificial

aurora [10]. In Sections 5-7 we show the results from multi-position bi-static HF Doppler radio-scatter observations of the radio-wave-modified ionosphere volume above the Sura facility. Section 5 discusses the spectral characteristics of signals scattered by artificial ionosphere turbulence when the pump frequency was close to the 4^{th} electron gyro harmonic. Sections 6 and 7 present multi-position bi-static HF Doppler radio-scatter observations of artificial field-aligned irregularities and recently discovered self-scattering phenomena [1]. We give summary and conclusions in Section 9.

2. Instruments and Techniques

The Sura facility belongs to and is operated by the Radiophysical Research Institute (NIRFI). The powerful radio wave transmitter is composed of three 250 kW transmitters. Each of these, if necessary, can be operated independently. The transmitter frequency can be varied from 4.3 to 9.5 MHz and may be changed step by step. This capability allows complicated programs to be run, such as, for example, stepping through the electron gyro harmonics. Phasing of the transmitters permits steering of the antenna beam within $\pm 40°$ from the zenith in the geomagnetic north-south direction. The full antenna beam is $12°\times 12°$ at 4.3 MHz, $10.7°\times 10.7°$ at 4.7 MHz and $9°\times 9°$ at 5.8 MHz for vertical pumping. Antenna gain is also frequency dependent, being equal to 80 at 4.3 MHz, 120 at 4.8 MHz and 150 at 5.8 MHz.

To monitor ionospheric conditions we ran the ionosonde (vertical sounding) about every 10 minutes. The ionosonde located at the Sura site was sensitive to the plasma frequencies above $1.75 \div 2$ MHz (corresponding to the plasma densities at the reflection level in the range 3.8×10^4 to 4.9×10^4 cm^{-3}) and up to 9 MHz (corresponding to the plasma density of about 10^6 cm^{-3} at the reflection level). A ground-based magnetometer located 30 km to the south-west from the Sura facility provided data on the geomagnetic field.

The campaign was equipped with an all-sky charge-coupled-device (CCD) camera (made by Keo Scientific Ltd.) from the NORSTAR project at the University of Calgary. The CCD camera used three interference filters, namely the 557.7 nm-filter with the bandwidth 2 nm, the 630.0 nm-filter with the bandwidth 2 nm, and a background (BGND) filter with the wavelength 541 nm and the bandwidth 2 nm. The software developed at Cornell University and used for operating the CCD imager allowed us to manually set any desirable sequence of filters and adjust the exposure time as needed.

In Fig. 1 we give a map showing the geometry of the observations. Three coherent scatter receiving sites located near Kharkov, Rostov and St. Petersburg were used to measure the signals scattered by the perturbed ionospheric volume above the SURA heater. For backscatter measurements we used what is now called the passive radar technique (for

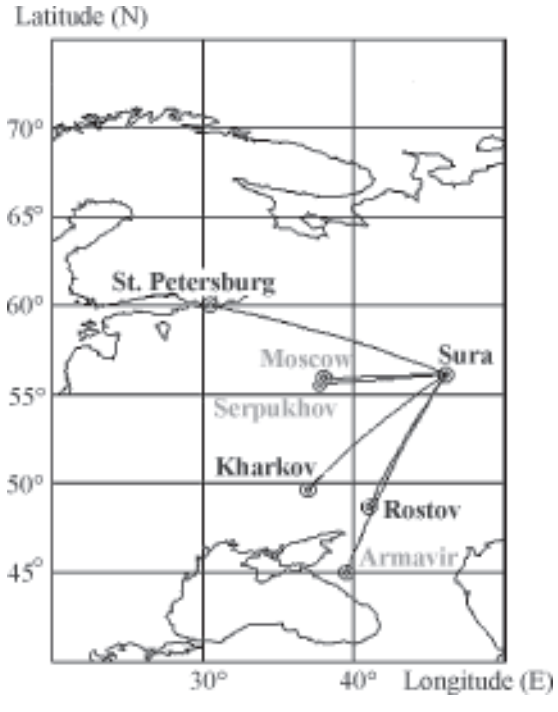

Fig. 1. *Geometry of the Sura experiment on August 10-20, 2004. Locations of the broadcasting stations and receiving sites are shown in grey and black, respectively*

details see [12-13]). To this end we chose the broadcasting stations near Moscow, Serpukhov and Armavir, whose CW signals (scattered by field-aligned irregularities which were induced by high-power radiowaves above the Sura facility) satisfied the Bragg resonant scattering condition to be registered at the four above-mentioned radar sites, thus allowing reconstruction of the 3D Doppler velocities inside the Sura-illuminated ionospheric volume.

For the first time in this kind of experiments, we supported optical observations with simultaneous plasma diagnostics using the so-called artificial periodic irregularities (API) technique [6].

In the second part of the campaign devoted to the F-region diagnostics we used a spectrum analyzer to observe stimulated electromagnetic emission (SEE) from the radiowave-modified ionosphere to determine such plasma parameters as, for example, the frequency of electron gyro harmonics. The real-time observations allowed prompt adjustments of the pump frequency in accordance with ionospheric conditions if necessary.

3. Artificial Periodic Irregularities

Artificial periodic irregularities (APIs) are generated in antinodes of the standing electromagnetic wave formed due to interference of the HF radio waves transmitted vertically and reflected from the ionosphere. The APIs are horizontally aligned with a vertical scale of one-half of the wavelength λ of the transmitted wave. When probed with radiowaves of the same wavelength, this weak API grid (imposed on the existing natural ionospheric structure) returns an enhanced signal from the altitudes occupied by natural plasma inhomogeneities, thus giving information about ionospheric structure up to the pump wave reflection level. The receiver and transmitter are located at the same site. There are two ways to satisfy the Bragg resonant backscatter condition, namely, [1] using the same frequency and polarization for the pump and probe waves and [2] using different frequencies.

As a rule, the API method uses the X-mode polarization to avoid inducing plasma instabilities. However, to combine optical observations with the API diagnostics, we had to use the O-mode polarization for both pumping and probing in order to have the maximum possible power for inducing optical emissions.

Among other advantages, the API method is capable of detecting sporadic ionization with plasma densities as low as about 1000 cm^{-3}, thus showing (more than an order of magnitude) better sensitivity than ionosondes. In the upper panel of Fig. 2, we show the E-region sporadic ionization (Es) as seen by the API technique on August 15-16, 2004 (during the daytime, no optics) as an enhanced backscattered signal and plotted as a function of local time and altitude (more details on producing altitude-time distributions of the scattered signal intensity using API technique can be found in [14]). In brief, the standing wave pattern produced by reflections from F-layer creates Bragg scattering targets which are more effective in the sporadic E-layers. In the lower panel we show three ionograms taken at times 18:28:05 LT, 18:45:41 LT and 20:29:44 LT. Here we created API using an X-mode polarization radiowave at the frequency 4.7003 MHz, which then was probed with X-mode waves at 4.7 MHz. From Fig. 2 it is clear that the ionosonde was capable of detecting reflected signals only when the amplitude of the API-scattered signal was near 50 dB or higher (the upper part of the double Es near 100 km altitude). For example, it did not register the signal backscattered from the low-altitude ionization layer at altitude near 80 km detected by the API technique.

The backscatter from the above-mentioned weakly ionized layer of ionization at altitude near 80 km registered on August 15-16, 2004 by the API method looks like mesosphere summer echoes (MSE) that have been registered at Sura using the API method many times, including simultaneous observations at 3 and 9 MHz [15]. These low-altitude ionization clouds caused radiowave focusing, thus providing enough energy to vibrationally ex-

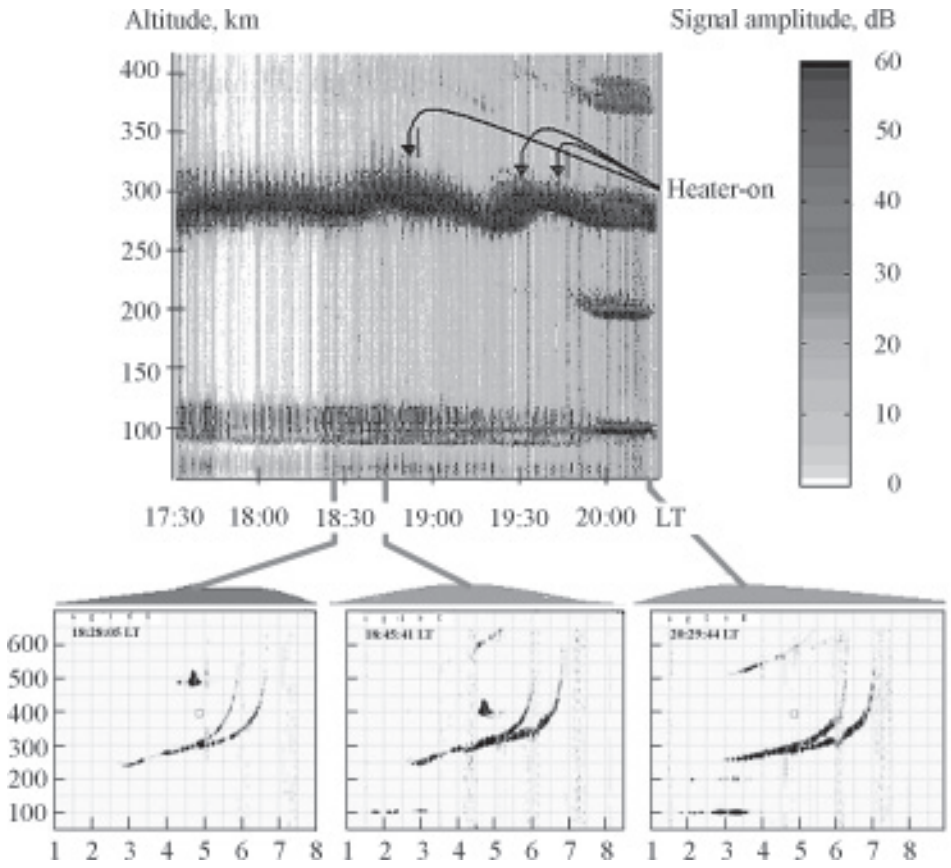

Fig. 2. *Altitude-time distribution of the scattered signal intensity (upper panel) reconstructed using the API data recorded from 17:30 to 20:30 LT on August 13, 2004. The O-mode heating was at 4.3 MHz with the pumping scheme 1 min on / 2 min off. APIs were formed and sounded by X-mode radiowaves at 4.7 MHz. The lower panel shows the ionograms taken from the Sura ionosonde sequentially (from left to right) at 18:28:05 LT, 18:45:41 LT and 20:29:44 LT*

cite hydroxyl molecules [10]. We will give more details on induced optical emissions in the next section.

Note that to effectively induce optical emissions the high-power radio waves of O-polarization and continuous heating schemes are used. To match this requirement and to be able to do simultaneous atmospheric diagnostics by the API technique we developed a special pumping/probing scheme shown in Fig. 3. We use the O-mode polarization for pumping (5 min on / 5 min off) and O-mode polarization of the same wavelength for probing during the heater-off periods. For 2 s after every 13 s of continuous heating during each 5-min heater-on period, we transmitted the 30-ms pulses (at a repetition frequency of 50 Hz) to probe the induced API structure. We use the usual probing scheme during the heater-off periods. Although we cannot run the complete API diagnostics using O-mode heating because of distortions caused by induced ionospheric instabilities, it is very important that O-mode heating is effective in detecting even relatively weak sporadic ionization. For example, it showed weak patchy-type Es pulsating near 80 km altitude during the night of August 15-16, 2005, when we observed radiowave-induced hydroxyl airglow (for details see [10]).

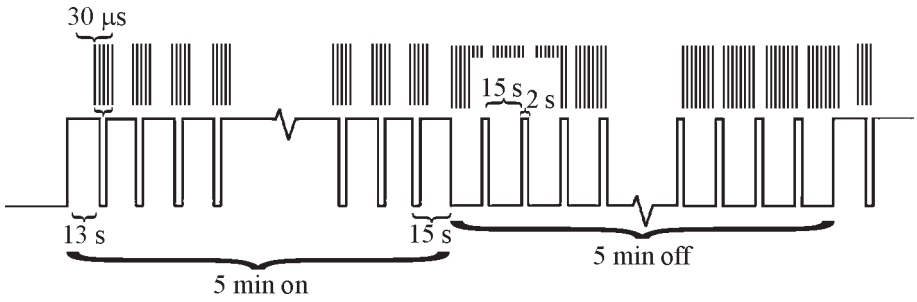

Fig. 3. *The scheme of API diagnostics that was used during dark time of the day simultaneously with optical observations*

Along with plasma and atmospheric diagnostics, the API observations were aimed at studying the effects of the ionosphere modification on the E-region sporadic ionization. Obviously, to make it efficient the Es critical frequency should exceed the pump frequency. These ionospheric conditions were at the end of the daytime API observations on August 15, 2004 (see Fig. 2). The respective ionograms show the strong overdense sporadic ionization near 100 km altitude and the API method additionally recorded a weaker sporadic E-layer just below it, near 90 km. Bakhmet'eva et al. [11] found that while the amplitude of the probing signal coming from 90 km remained unchanged, the amplitude of the signal from 100 km was decreasing with heating (the heating did not noticeably affect the API relaxation time). The reasons for such a difference are not yet understood. A possible explanation may be related to the difference in the magnitude of the electric field of the radiowaves at the two altitudes and the influence of heating on ionospheric irregularities, for example the triggering of different instability mechanisms at different altitudes. Frolov et al. [16] showed that for a patchy type Es the intensity of the backscattered signal increased with heating and induced signal fluctuations appeared. Clearly, high-power radiowaves can modify sporadic ionization, but to understand how and why this modification takes place requires further experimental and theoretical investigation.

4. Optical Observations

Artificial airglow occurs when, due to the interaction of a powerful electromagnetic wave with the ionospheric plasma, electrons acquire enough energy for collisional excitation of neutral species. The most frequently observed artificial emissions occur when excited atomic oxygen in the $O(^1D)$ state relaxes to the ground state, emitting a photon with a wavelength of 630.03 nm (the excitation energy is 1.97 eV). This emission comes from altitudes 250 ± 50 km and may be accompanied by a significantly weaker F-region green-line emission of atomic oxygen (because of a higher excitation energy, 4.19 eV, compared to that of the 630.0-nm airglow), which occurs when atomic oxygen in the $O(^1S)$ state relaxes and emits a photon with a wavelength of 557.7 nm.

All three preceding campaigns at the Sura facility involving optics (in 1990, 1993 and 1995) were aimed at measuring the F-region airglow in 630.0-nm emission from atomic oxygen in the $O(^1D)$ state and at using these measurements for determining plasma drifts, neutral winds, diffusion coefficients, and collisional quenching times [17-18]. Bernhardt and coauthors did not observe green line emission of atomic oxygen at 557.7 nm. Concerning the F-region 557.7-nm radiowave-induced airglow, most probably Bernhardt and co-authors did not observe it because there were not enough accelerated electrons with sufficiently high energy to excite a detectable

airglow. Neither of these three campaigns was aimed at measuring the E-region airglow, since it had not yet been discovered, and therefore the experiments were carried out when there was no E-region sporadic ionization.

In the F-region study-oriented part of our August 2004 campaign, we investigated the 630.0-nm optical signatures of the radiowave pumping toward the geomagnetic zenith, which for the Sura location was predicted to be the most effective for transmissions at the 12° geomagnetic south [19-20]. Because the weather was not favorable for optical observations, we were unable to accomplish the planned program. However, the observations were performed for two days, specifically on August 13 (vertical heating) and August 20 (pumping toward the magnetic zenith by heating at the 12° angle), when the ionospheric conditions were very similar (the F-maximum critical frequency in both cases was 5.8 MHz) as well as the effective radiated power of about 120 MW and the heating schedule 5 min on / 5 min off in both cases. The heating frequency was 4.7 MHz on August 13, 2004 and 4.7853 MHz on August 20, 2004. The angular dimensions of the heater beam for these two days were also very close, namely 10.7° E-W by 10.7° N-S for the vertical heating and 10.7° E-W by 11.1° N-S for the heating at the 12°-south angle in the geomagnetic coordinates. According to the ionosonde observations, the pump wave was reflected from the virtual height of about 330 km in both cases.

In Fig. 4 we show two images of the F-region 630-nm induced airglow unwarped at 300 km altitude (a) for vertical radiowave transmission (22:33:47 LT on August 13, 2004; the heater was on for 167 s) and (b) for transmission at the angle of 12° to the geomagnetic south in order to radiate the electromagnetic power toward the magnetic zenith (22:13:57 LT on August 20, 2004; the heater was on for 177 s). The exposure time for both images was 30 s. We also took 30 s back-

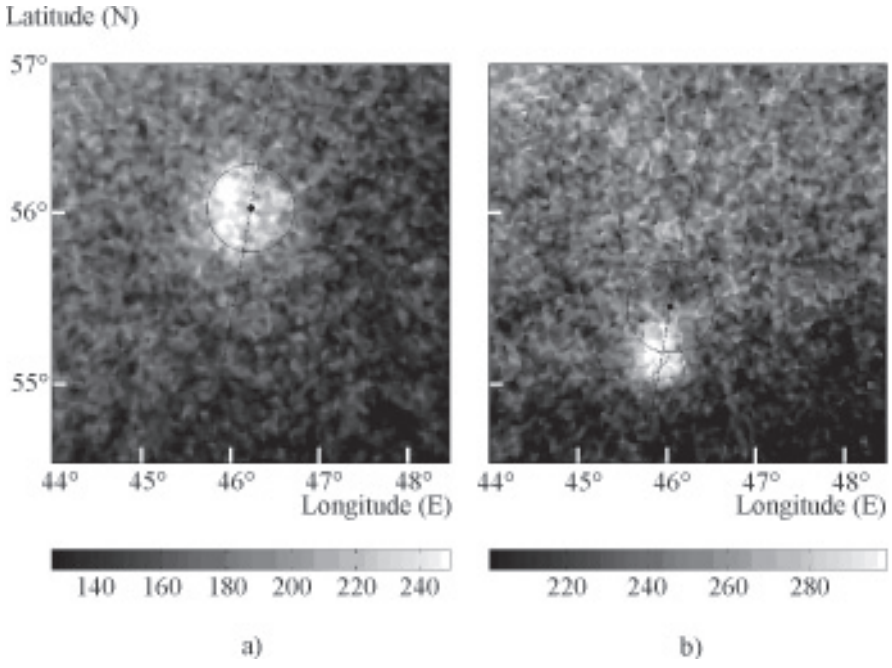

Fig. 4. *All-sky images of the F-region 630-nm induced airglow unwarped at 300 km altitude (a) for vertical radiowave transmission (22:33:47 LT on August 13, 2004; the heater was on for 167 s) and (b) for transmission at an angle 12° to the geomagnetic south (22:13:57 LT on August 20, 2004; the heater was on for 177 s). The intensities are given in Rayleighs*

ground exposures (off-band) to correct the 630.0-nm images after applying a star removal algorithm to both background and red line images. We mark the center of the heater beam with the dot. We impose a geomagnetic meridian and show the location of magnetic zenith by the cross to make it easier to identify the location of the 630.0-nm artificial airglow for heating at the $12°$ angle. One can clearly see that on August 20 the center of the induced airglow cloud lies on the geomagnetic meridian to the geomagnetic south from the center of the heater beam, indicating that the radiowave energy was going about $1 \div 2°$ off the magnetic zenith (note that the dip angle at the Sura location is $71°$).

The width of the airglow spot in this case was about one half of that for vertical heating observed on August 13, 2004. We are planning to analyze these data in more detail, although preliminary analysis of sequential images shows that (i) for well-developed airglow the maximum of relative intensity was more than twice as high for heating at the $12°$ angle than for vertical case, and (ii) the center of the airglow cloud for the oblique heating seems to appear at a longer distance from the geomagnetic zenith and then to move closer to it with heating going on.

The E-region radiowave-induced airglow was discovered recently, and the two types observed are the 557.7-nm emission from atomic oxygen [3-4] and the red hydroxyl aurora (this campaign, [10]). Both types are associated with sporadic ionization. While the $O(^1S)$ 557.7-nm airglow was a footprint of the overdense E-region sporadic ionization (E_s) (the pump frequency was less than the Es critical frequency) [4], the red hydroxyl aurora was a result of radiowave focusing by low-altitude ionization clouds near 80 km altitude (the pump frequency was higher than the Es critical frequency) [10]. A schematic illustration of the two mechanisms may be found in [21]. As we have already mentioned in Section 3, the density of these low-altitude ionization clouds was not high enough to be detectable by the Sura ionosonde but was registered with the method of artificial periodic irregularities (API) [6] using the diagnostic scheme of simultaneous optical and API observations suggested in [5]. The key point in these observations is that the light detected in a 2 nm wide filter centered on 630 nm was seen quite soon $(1 \div 2\ \text{s})$ after launching the radiowaves. This short response time rules out the 630 nm emission origin from atomic oxygen, since it has a rise time of about 30 s [22].

We successfully induced the 557.7-nm airglow from the atomic oxygen in the $O(^1S)$ state. However it was much weaker than we observed in Arecibo [4] and did not exceed 10 Rayleighs on all occasions. The sporadic ionization in all these cases had a critical frequency exceeding the pump frequency and was located near 110 km altitude. Similarly to atmosphere clouds, the ionization clouds sometimes could be of a quite unusual shape. As an example, Fig. 6 in [11] presents a 557.7-nm image of patchy sporadic ionization of a V-shape pointing to the west with a size of the shoulders of 10 by 3 km and 9 by $1 \div 1.5$ km (Es critical and blanketing frequencies were 5.4 and 2.7 MHz, respectively) observed at 23:04 LT on August 19, 2004.

5. Spectral Characteristics of Backscatter from Artificial Ionospheric Turbulence when the Pump Frequency is Close to the 4th Electron Gyro Harmonic

The second part of the campaign was predominantly aimed at studying radiowave-induced processes in the upper atmosphere (the ionosphere F-region), the artificial ionosphere turbulence (AIT) in particular, using simultaneous diagnostics of the heated ionospheric volume by multi-position backscatter measurements and by the method of stimulated electromagnetic emission (SEE). Multi-position backscatter observations give information on the dynamics of artificial small-scale irregularities (field-aligned irregularities with a field-perpendicular scale less than about 50 m) and drifts in the heated volume [7-9], while the SEE measurements allow us to experimentally find the frequency of the electron gyro harmonics [23]. The latter are seen

as a complete depression of the down-shifted maximum component in the SEE spectrum when the pump frequency is close to the frequency of the electron gyro harmonics.

Recent SEE experiments have shown that the AIT properties in the perturbed ionospheric volume change significantly when the pump frequency lies in the $100 \div 200$ kHz vicinity of the frequency of the electron gyro harmonics [24-28].

Backscatter spectra were found to broaden from fractions of Hz during AIT development and relaxation to several Hz at the stage of well-developed turbulence [29]. Koloskov et al. [30] showed that the splitting of the Doppler spectra of backscattered signals into a series of well-defined harmonics was caused by induced plasma heating by radial drifts inside the heated volume. Alternatively, the splitting may be due to a radial electric field causing rotation about the heated volume [29]. Indeed, [31] have reported quasi-dc electric fields created inside a heated volume. Yampolski and coauthors [9, 12] discovered the $20 \div 150$-s quasi-periodicity in Doppler shifts of backscattered signals and its correspondence to Pc $3 \div 4$ magnetic pulsations. Ponomarenko et al. and Honary et al. [32, 33] observed that when the pump frequency was close to the 4th gyro harmonic, in addition to depression of the downshifted maximum and broad continuum components in the SEE spectra, there was a minimum of the backscatter intensity accompanied by SEE spectra broadening for the pump frequency slightly exceeding the 4th gyro harmonic compared to the case when the pump frequency was slightly less than the 4th gyro harmonic. The magnitude of spectral broadening depended on the pump power. The transition from broad to narrow spectra after the pump turn-off took no more than $50 \div 70$ ms and it took 10 to 20 s for these narrow spectra to relax.

To understand the above-mentioned broadening of Doppler spectra near the 4th gyro harmonic on August 19, 2004 (15:00-17:00 UT), we observed backscatter from the radiowave-modified ionospheric volume over the Sura heating facility using the so-called "passive radar" technique. Three radio systems (including the UTR-2 radio telescope) located near Kharkov, St. Petersburg, and Rostov were registering signals from the Time Service station RWM (Moscow) operating at 9.996 and 14.996 MHz that, according to the Bragg resonance conditions, were backscattered by radiowave-induced field-aligned irregularities with field-perpendicular scales of 16 and 11 m, respectively.

The Sura facility allows pumping at frequencies close to those of the 4th to 7th electron gyro harmonics. The electron gyro frequency above Sura is $f_{ce} \approx 1.3 \div 1.35$ MHz. We vertically transmitted the O-mode polarized waves with an effective radiative power $\mathrm{ERP} \approx 150$ MW. The frequency of the electron gyro harmonics (the 4th one in this case) was determined from the depression of the downshifted maximum [23, 34] and the properties of the broad upshifted maximum [27] in the SEE spectra at the double resonance when the pump frequency $f_{\mathrm{pump}} \cong f_{\mathrm{uh}} \cong 4 f_{ce}$ (f_{uh} is the upper hybrid frequency and $4 f_{ce}$ is the frequency of the 4th electron gyro harmonic at the level of the upper hybrid resonance). The SEE method was capable of detecting $4 f_{ce}$ with an accuracy better than 5 kHz.

We started each observational cycle by finding $4 f_{ce}$. Based on the ionospheric conditions we then chose a frequency range of about $80 \div 100$ kHz enveloping $4 f_{ce}$ for radiowave transmissions and step-by-step changed the transmitter frequency with a 20 kHz step. The transmitter at each sequential pump frequency was 105 s on / 15 s off. The pause for 15 s provided enough time to switch to the next pump frequency. Such a diagnostic scheme allowed obtaining information on the temporal evolution of the scattered signal intensity with optimum spectral resolution in the backscatter measurements.

During each cycle of the above-mentioned frequency scanning we kept diagnosing ionospheric conditions with the SEE observations to follow variations in the electron gyro frequency caused by changes in natural ionospheric conditions. This allowed us to promptly correct the magnitude of $4 f_{ce}$ and to determine the frequency range for the next scanning cycle. The duration of one observational cycle was

about $10 \div 12$ min. From 15:00 to 17:00 UT we ran in total 8 observation cycles.

The day of August 19, 2004 was geomagnetically quiet with $K_p \approx 1$.

Figure 5 presents examples of dynamic spectra of signals scattered by the 11- and 16-m irregularities recorded near Kharkov at 14.996 and 9.996 MHz from 15:59 to 16:10 UT ($4f_{ce} \approx 5.36$ MHz, the scanning range was $5.34 \div 5.44$ MHz). It is clear that a noticeable spectral broadening occurred when the pump frequency was close to or above $4f_{ce}$.

The backscatter from 11- and 16-m artificial field-aligned irregularities is seen as having two components (narrow and wideband) distinguished by their relaxation times and dependence on the pump frequency. The effect of backscatter spectral broadening is clearly seen in both the narrow and wideband backscatter components near $f_{pump} \cong 4f_{ce}$, reaching its maximum at a frequency offset $f_{pump} - 4f_{ce} = 20 \div 40$ kHz which corresponds to the most effective generation of the second component in the broad upshifted maximum in the SEE spectra and to the most effective excitation of the electron Bernstein modes [27]. The spectrum broadening decreases with a further increase of $f_{pump} - 4f_{ce}$. The narrowband backscatter component carries the major part of the backscatter power, which is about an order of magnitude higher than the wideband one.

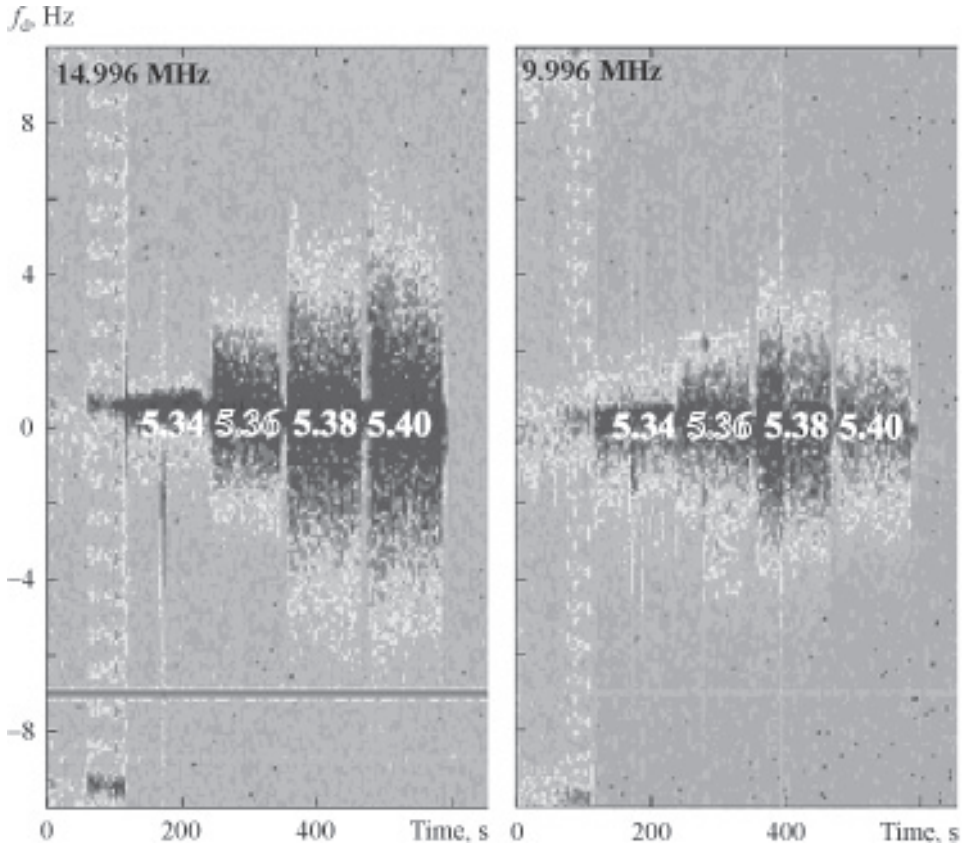

Fig. 5. *Doppler spectra of the scattered signals recorded by the N-S array of UTR-2 in Kharkov at 14.996 and 9.996 MHz (corresponding to the field-aligned irregularities with field-perpendicular scales 11 and 16 m) from 15:59 to 16:10 UT (UT=LT + 4 h) on August 19, 2004. The heater frequency was changed sequentially from 5.34 to 5.40 MHz with a step of 20 kHz. The transmitter at each sequential pump frequency was 105 s on and 15 s off. The 4th gyro harmonic frequency was about 5.36 MHz*

We estimate the growth time t_1 of the broad-band component after the pump switch-on and its relaxation time t_2 after the pump switch-off as $t_1 = 0.5 \div 1$ s and $t_2 \le 1$ s. This relaxation time is significantly shorter than the relaxation time of the $11 \div 16$-m irregularities generated by the radiowaves with the frequencies far from the electron gyro harmonics, which is about $10 \div 15$ s [29, 35]. Therefore the broadening of the backscatter spectra at pump frequencies close to the 4th electron gyro harmonics seems to be caused by the radiowave-induced random motions of scatterers inside the perturbed ionospheric volume rather than due to irregularity drift, which would shift the backscatter spectrum as a whole. The velocity of these random motions may reach 100 m/s and is independent of the scatterer scales. Ponomarenko et al. [32] explained these motions by excitation of the electron Berstein modes. An alternative explanation may be excitation of irregularities that move not so markedly along the magnetic field as is usually the case. Then the diffusion coefficient would be greater, the lifetime shorter and the Doppler spread, which is inversely proportional to the lifetime, would be greater. Rocket observations in the presence of a pump wave revealed irregularities with short parallel wavelengths at the heights where the local plasma frequency was equal to an electron gyro harmonic, suggesting generation of electron Bernstein modes and possibly lower-order hybrid waves which have a finite field-aligned wave number [36]. Note that while the pump in this rocket experiment was not matched to an electron gyro harmonic, nonetheless irregularities formed at altitudes which were not related to the reflection heights.

6. Multi-Position Bi-Static HF Doppler Radio-Scatter Observations of Artificial Field-Aligned Irregularities

To study dynamics in the HF-illuminated volume we used signals from three broadcasting stations located in Moscow (55.80° N, 38.30° E; the distance to Sura was 490 km; the operating frequencies were 14.996, 9.996 and 12.070 MHz), Serpukhov (55.00° N, 37.50° E; the distance to Sura was 550 km; the operating frequency 11.630 MHz) and near Armavir (45.00° N, 39.50° E; the distance to Sura was 1320 km; the operating frequency 15.455 MHz). The broadcasting HF signals were scattered by the $10 \div 15$-m irregularities generated by high-power radiowaves above the Sura facility and were received at three sites located near St. Petersburg, Kharkov and Rostov (see the map in Fig. 1). The Doppler spectrum technique was used for analyzing the fine structure of the scattered signals. Viewing line-of-sight Doppler velocities from different angles allowed reconstructing the temporal behaviour of the 2D velocity of the scatterers in the radiowave-illuminated volume.

We observed diagnostic signals scattered from artificial field-aligned irregularities (AFAIs) during most of the high-power radiowave transmission sessions. The intense scattered signals were simultaneously registered at the three receiving sites on August 13, 15, 17, 18, 19, and 20. As an example, Fig. 6 presents dynamic Doppler spectra (sonograms) obtained on August 20, 2005 from 18:20 to 19:30 UT for the Armavir–Sura–St. Petersburg ($f = 15.455$ MHz; top panel), Serpukhov–Sura–Kharkov ($f = 11.630$ MHz, east-west and north-south subarrays of the UTR-2; upper and lower middle panel, respectively), Serpukhov–Sura–Rostov ($f = 11.630$ MHz; bottom panel) and Moscow–Sura–Rostov ($f = 14.996$ MHz; bottom panel) paths. A signature of HF-induced field-aligned irregularities is seen as additional tracks shifted from zero Doppler frequency corresponding to the direct signal propagating from the transmitter to the receiver along the great-circle path. From Fig. 6 one can see that scattered signals were observed during all heater-on periods shown with bars along the UT axis.

From multi-position bi-static Doppler scatter observations it is possible to estimate the magnitude and direction of plasma motion velocities in the HF-induced ionospheric patch. Calculations for the model described in [37] showed that from 18:20 to 19:30 UT on August 20, 2004, AFAIs were moving in the

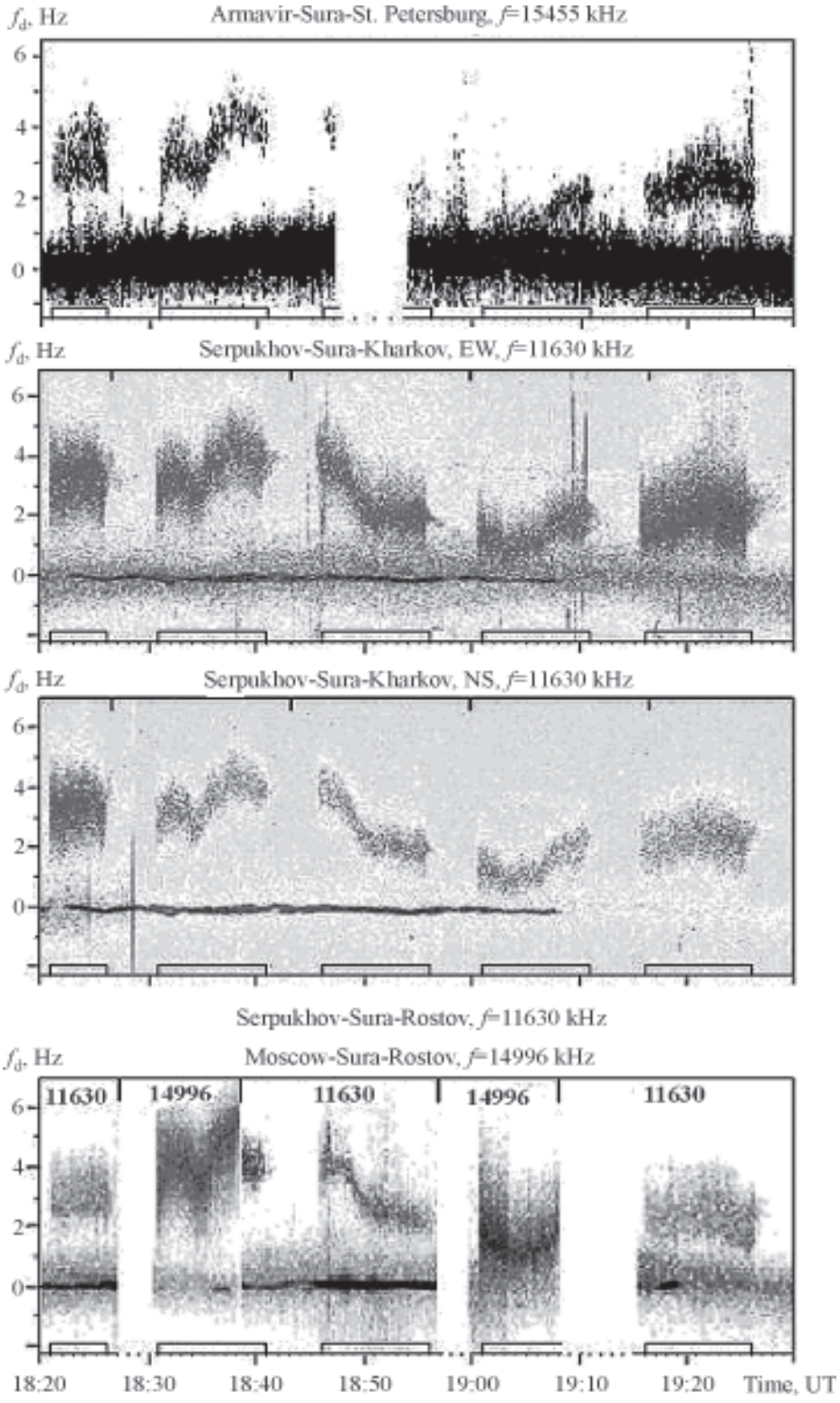

Fig. 6. *Dynamic Doppler spectra of HF broadcasting signals observed from 18:20 to 19:30 UT on August 20, 2004 at radio paths Armavir–Sura–St. Petersburg at 15.455 MHz (top panel); Serpukhov–Sura–Kharkov path at 11.630 MHz with EW (upper middle panel) and NS (lower middle panel) subarrays of the UTR-2; and Serpukhov (Moscow)–Sura–Rostov path at 11.630 and 14.996 MHz (bottom panel). For each path the direct signal propagating from the transmitter to the receiver along a great circle corresponds to the zero Doppler frequency shift. The intervals of high-power radio transmissions are marked by bars on the time axis*

south-west direction (the azimuthal sector of $210°$ to $250°$ counted clockwise from the North). From Doppler measurements we found the magnitude of AFAI velocity to be varying from about 50 to 150 m/s. Note that the day of August 20, 2004 was geomagnetically perturbed with $K_p = 3 \div 4$. A similar reconstruction for the previous day, August 19, 2004, that was geomagnetically quiet ($K_p \approx 1$), gives a north-eastward motion (the azimuths between $30°$ and $60°$) of the AFAIs with much more modest velocities of 30 to 70 m/s. These results are in good agreement with the current ideas about the penetration of magnetospheric processes to middle latitudes. For example, [38] found that at very low K_p the zonal drifts at Millstone Hill Observatory were small and eastward oriented, while at modest K_p's they were westward. This could be due to penetration of the convection electric field or because of disturbances in the dynamo region produced by winds blowing out of the polar cap/auroral oval.

The most prominent feature in the observed line-of-sight velocities (Doppler frequencies f_d) of the artificial field-aligned irregularities is their wavelike behavior presenting a wide spectrum of wave processes. The oscillations in Doppler frequency shifts showed two types of wave processes. The first one is a relatively slow process with periods between 10 and 45 min, which is close to the periodicity of medium-scale traveling ionospheric disturbances caused by atmospheric gravity waves. The amplitude of these oscillations was about 2 to 5 Hz. These relatively slow f_d variations were often modulated by shorter-period wave processes with periods of 30 to 60 s and amplitudes of $0.5 \div 1$ Hz, which corresponds to the Pc $3 \div 4$ magnetic pulsations.

The pulsations with periods $20 \div 80$ s in the intensity of signals scattered by artificial irregularities above the Sura radio transmitter have been routinely observed earlier [7-8, 39, 40]. During the second part of the campaign we modulated the power of one of the Sura transmitters using the scheme 15 s on / 15 s off to artificially induce Pc3 geomagnetic pulsations. Some of our attempts were successful and we observed quasi periodic variations in Doppler frequency shifts around the transmitted frequency with the same period of 15 s and amplitude up to 0.5 Hz. We are going to discuss these results in more detail in the near future.

Another feature of the signals scattered by radiowave-induced irregularities is the splitting of the scattered signal into two (or sometimes three) components, which effect was already mentioned in Section 5 above (see, for example, cycles 18:21-18:26 and 19:16-19:26 UT in Fig. 6). This effect has been observed in both midlatitude [30] and highlatitude ionosphere [41]. Koloskov et al. [30] saw a possible explanation of the phenomenon in the radial drift of artificial irregularities from the center of the heated volume.

Based on the rocket measurements during the heating experiment in Arecibo [42] that revealed the presence of several altitude-separated regions of artificial small-scale irregularities, [43] supposed that a temperature-gradient-driven instability such as the drift wave could be responsible for the patches of heater-induced striations at different heights. The question is still open and to answer it more observations are needed.

Finally, we would like to note that (i) during some of the HF transmitting sessions when the Sura ionosonde observed intense sporadic ionization in the E-region and no F-spread (as, for example, from 17 to 18 UT on August 18 and from 19 to 20 UT on August 19), the signals scattered by the artificial field-aligned irregularities in the F2-layer showed strong spectral broadening in the Doppler sonogram; and (ii) we successfully excited Alfven waves using ± 15 s modulation and pumping toward the geomagnetic zenith (transmitting at $12°$ to the south) on August 19, 2005.

7. Multi-Position Observations of the Self-Scattering Effect

The self-scattering effect was discovered during the 2002 campaign when the high-power radio signals radiated by the Tromsø heating facility were scattered by the irregularities it had induced in the heated volume [1].

The distinctive feature of the self-scattering compared to any backscattering is its wide angular indicatrix. This allows observing the scattered radio signal from different locations corresponding to propagation paths of different lengths and orientations. Coherent reception and spectral analysis of the self-scattered signals were performed simultaneously near St. Petersburg (Russia), Kharkov (Ukraine) and at the Ukrainian Antarctic station "Academician Vernadsky". Along with regular narrow-band signals at the pump frequency (associated with radiation from side lobes of the heater antenna) we observed wide-band components which were well correlated in intensity and Doppler frequency shifts (as a rule of several Hertz in magnitude) at all the receiving sites. Such a similar behavior allowed us to suppose that the Doppler variations were produced by the processes inside the heated volume. Since this is the only common volume for all radio paths, natural processes generated by electric fields, neutral winds, atmospheric gravity waves, magneto-hydrodynamic waves, etc. inside the heated volume may cause changes in the radiowave-induced irregularities, thus resulting in a similar modulation of the scattered signals at different radio paths.

The exciting discovery of the self-scattering effect [1] triggered several questions which we made an effort to clarify during the Sura campaign in August 2004. The primary issues were (i) the mechanism of radio signal scattering over a large range of azimuthal angles that assumed a horizontal isotropy of the scattering irregularities; (ii) the nature of the motions causing synchronous variations in the Doppler frequency shifts and in the intensity of the scattered signals at very distant receiving sites; and (iii) the relation between the variations in the self-scattered signal and the signals scattered by small-scale radiowave-induced irregularities.

In addition to the observations of scattered signals at the pump frequency f_{pump} (as in the Tromsø campaign), we simultaneously tried monitoring the scattered spectra at the second harmonic of the pump frequency, $2f_{\text{pump}}$. Synchronous registration of the three components of geomagnetic field variations near the Sura heating facility allowed us to correctly identify the nature of motions inside the heated volume. As usual, we routinely monitor the critical frequency of the ionosphere from ionosonde measurements.

Shown in Fig. 7 is an example of dynamic spectra of the self-scattered signals at the first harmonic of the pump frequency observed near St. Petersburg (the radio path is 963-km long) and Kharkov (the radio path is 994-km long) (see panels b and a, respectively), at the second harmonic of the pump frequency observed near St. Petersburg (panel d) and synchronous variations of one component of the Earth's magnetic field (panel c). A cross-correlation analysis of the Doppler frequency shifts in the self-scattered signals showed their high correlation with geomagnetic variations, with the maximum of the cross-correlation coefficient about 0.65. This allows suggesting that (i) the signals at both radio paths were indeed scattered over the Sura heating facility and (ii) the motion of the ionospheric plasma was due to crossed electric and magnetic fields associated with MHD processes and therefore the velocity of the stimulated irregularities was modulated by geomagnetic field variations.

Concerning the nature of variations in the Doppler shifts of the self-scattered signals, two possible mechanisms can be suggested. The first one is true physical motions of the scattering irregularities. In this case

$$f_{\text{d}} = V_{\text{s}} f_{\text{s}}/c,$$

where V_{s} is the projection of the scatterer velocity on the scattering direction, f_{s} is the carrier frequency of the scattered signal (in our case f_{s} was equal to f_{pump} or $2f_{\text{pump}}$) and c is the velocity of light. The second mechanism consists in variations of the refraction index $n(l)$ along the radio propagation path. Then

$$f_{\text{d}} = \frac{f_{\text{s}}}{c}\frac{\partial}{\partial t}\int_L n(l)\,\text{d}l.$$

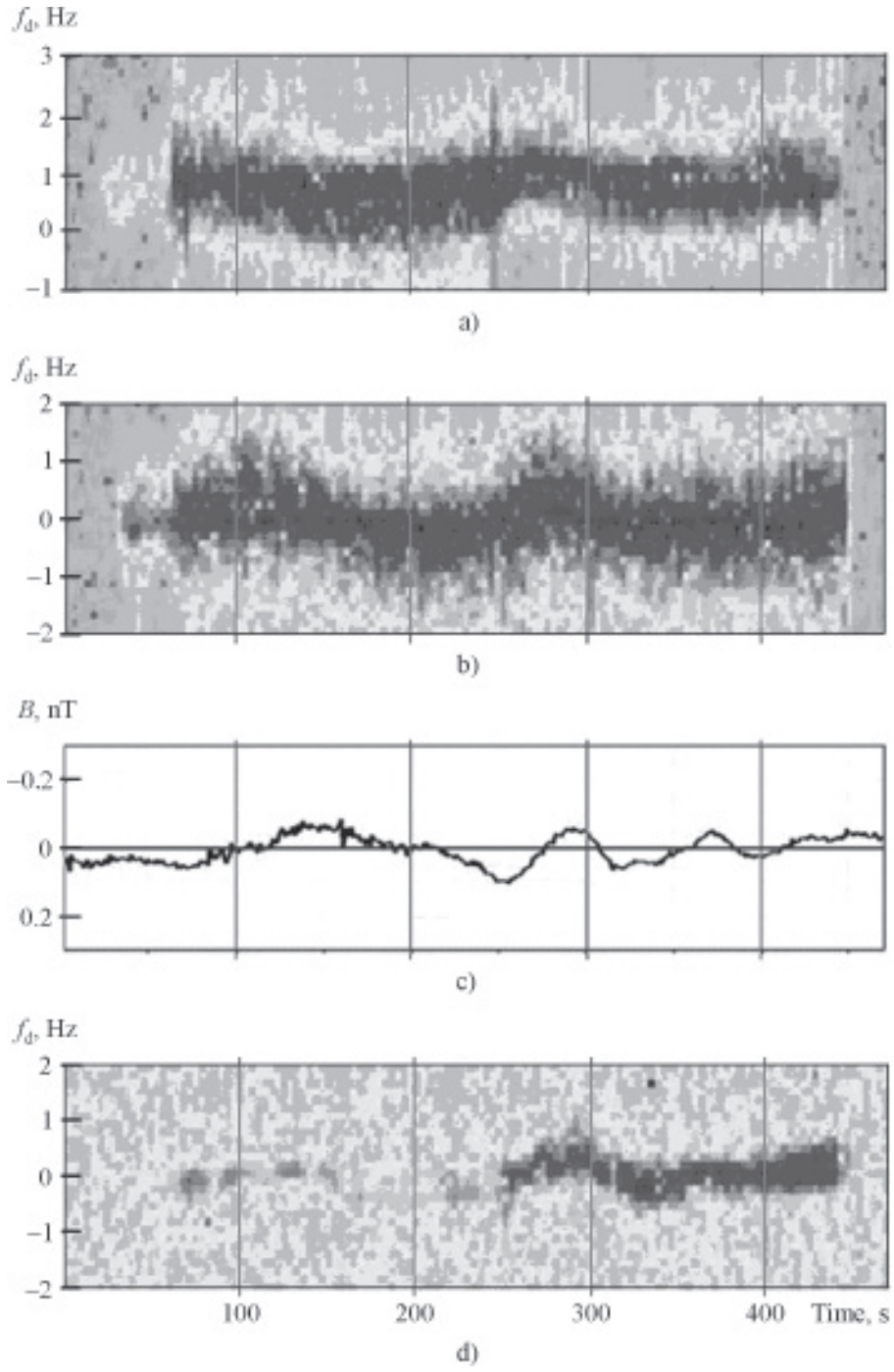

Fig. 7. *Spectrograms of "self-scattered" signals observed at RAO between 17:57 and 18:05 UT at the first harmonic of the heater (a), and at the first (b) and second (d) harmonics at AARI. Panel c presents geomagnetic field variations (H_y – component) measured close to the Sura heater*

The two mechanisms follow different frequency dependences. The f_d variations are proportional to f_s in the first case, while are inversely proportional to f_s in the second case. Either of the two mechanisms could work. However, our analysis of simultaneous

observations of the self-scattering effect at the first (Fig. 7, b) and the second (Fig. 7, d) harmonics of the pump frequency shows that the refractive mechanism dominates. Indeed, the maximum variation of f_d of self-scattered signals at $2f_{pump}$ was about one half of that at f_{pump}.

This suggests that the upgoing trajectory segment from the heater to the scattering volume, which is common for all the radio paths, is the major contributor to the Doppler shift variations. Therefore the magneto-hydro-dynamic (MHD) process modulates not only the position of irregularities inside the scattering volume but also the electron density above the high-power radio source.

In Fig. 8 we show an example where modulation of the scattered signals was caused by MHD processes. One can clearly see that the Doppler velocities (in m/s) estimated from the Doppler frequency shifts f_d of the self-scattered signals at 4.785 MHz recorded simultaneously near St. Petersburg (curve 1) and Kharkov (curve 2) are well correlated with each other and with the geomagnetic variations (curve 3). Variations in the Doppler velocity and intensity of the aspect-scattered signal at 11.630 MHz as observed near Kharkov are shown by curves 4 and 5, respectively.

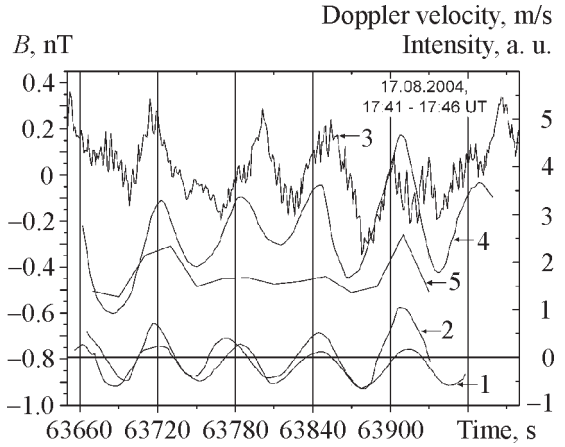

Fig. 8. *Doppler velocities estimated from Doppler frequency shifts of the self-scattered signals at 4.785 MHz recorded simultaneously near St. Petersburg (curve 1) and Kharkov (curve 2), and variations of the H_x-component of the geomagnetic field measured close to the Sura heater (curve 3). Shown by curves 4 and 5 are variations in the Doppler velocity and intensity of the aspect-scattered signal at 11.630 MHz as observed near Kharkov*

Understanding the formation of a self-scattered signal in the perturbed ionospheric volume requires reconstructing the 3D structure of the high-power radio wave near its reflection level. The task is extremely difficult. Obviously, there are two factors that should be taken into account, namely the regular structure of artificial periodic irregularities below the reflection level produced by the incident and reflected waves and stochastic irregularities associated with the plasma turbulence inside the heated volume. We will present the corresponding model calculations in our future publications. Comparison of the model with observations would allow using the effect of self-scattering for diagnostics of the spatial structure of the high-power radiowave and 3D spectra of the radiowave-induced irregularities. We expect to obtain further insight into the self-scattering effect from a comparative analysis with API observations where we used the diagnostic scheme (see Fig. 3) specifically developed for O-mode continuous heating in order to induce optical emissions. For understanding the generation mechanism of the self-scattering at the second harmonic of the pump frequency, further purposeful experimental studies are required.

8. Summary and Conclusions

This paper is aimed at giving an overview of the optical-backscatter-heating campaign which was conducted on August 10-20, 2004 rather than at presenting several detailed case studies that will be the subject of separate publications. We believe that our campaign was so successful because of two major factors: (i) properly chosen time of campaign to have the best possible combination of the sporadic E occurrence and dark time required for optical observations at the highest possible maximum plasma density of the ionosphere, and (ii) simultaneous observations by

different instruments and methods. For example, in order to make use of several diagnostic methods (as, for example, optical and API) we developed the scheme of the API diagnostics shown in Fig. 3, based on O-mode probing during O-mode continuous heating. Despite the fact that such a scheme is significantly less effective than the classical one [6], it served well to the purpose of observing weak sporadic ionization which would be undetectable by the ionosonde. We also expect that this regime of the API method, as well as processing the self-scattered signals recorded at the Ukrainian Station "Academician Vernadsky" in Antarctica, will give a further insight into the self-scattering effect.

Below we briefly summarize the main results from our optical-backscatter-heating campaign at the Sura facility on August 10-20, 2004.

Optics and API

– Discovery of radiowave-induced red $OH(9\div3)$ Meinel band emission caused by ray focusing due to weak (underdense) sporadic ionization near $80\div85$ km altitude [10];

– Es-associated 557.7-nm radio-induced airglow from $O(^1S)$ [11];

– pumping the radiowave energy toward the geomagnetic zenith by transmitting at a $12°$-to-the-south angle from the vertical accompanied by 630.0-nm emissions from $O(^1D)$ and offset of these optical emissions by $1\div2$ degrees from magnetic zenith;

– natural bore wave observed in red $OH(9\div3)$ and 557.7-nm from $O(^1S)$ (to be submitted as a separate paper).

Backscatter

– Reconstruction of the temporal behavior of the 2D velocity vector of the radio wave-induced irregularities in the heated volume [44];

– Alfven Wave generation using ±15 s modulation and pumping toward the geomagnetic zenith (transmitting at $12°$ to the south);

– long-lasting "independent" life of the backscatter signal after the pump turn-off which most probably is associated with sporadic ionization $(18:00\div18:20)$ UT on August 13, 2004);

– splitting of the Doppler spectra of the scattered signal into two (sometimes three) components [41];

– two well-distinguished components (narrow- and wide-band) in the Doppler spectra of the scattered signal with the narrow component being more intensive than the broad one by a factor of 10 [44-45];

– broadening of the frequency spectrum of the artificial ionosphere turbulence when the pump frequency was close to the 4^{th} electron gyro harmonic with a maximum spectral width at the frequency offset of about $20\div40$ kHz [45]. We have proved that the effect of spectral broadening was not caused by the irregularity drift in the heated volume.

The self-scattering effect [2]

– First observations of self-scattered signals at the second harmonic of the pump frequency that allowed pinning down the refractive mechanism of Doppler variations;

– first observations of synchronous variations in backscattered and self-scattered radio signals;

– establishing the correlation of the self-scattered signal with the magnetic field fluctuations.

We are going to give more detailed presentations of case studies in separate publications to follow.

Acknowledgments. This work has been supported by Grant ATM-0000196 from the Atmospheric Science Section of the National Science Foundation. LMK's work has been supported via a contract with Cornell University and by the Canadian Natural Sciences and Engineering Research Council. ED and TST acknowledge the Canadian Space Agency for their support of NORSTAR through the Canadian GeoSpace Monitoring Program. The work has been supported in part by Russian Foundation of Basic Research grants 04-05-64140, 05-05-64304, 05-02-16493 and 04-05-64160, 02-05-65281, INTAS grant 03-51-5583 and CRDF grant 1334-NO-2. The authors thank Drs. D. S. Kotik and S. V. Polyakov of NIRFI and Dr. B. Klain of the Borok Observatory for providing the magnetometer data.

References

1. A. V. Zalizovski, S. B. Kashcheyev, Yu. M. Yampolski, V. G. Galushko, V. S. Beley, B. Isham, M. T. Rietveld, C. La Hoz, A. Brekke, N. F. Blagoveschenskaya, and V. A. Kornienko, "Spectral Features of HF Signals from the EISCAT Heating Facility in Europe and in Antarctica", *Radio Physics and Radio Astronomy*, vol. 9, No. 3, pp. 261-273, 2004.
2. Yu. M. Yampolski, A. V. Zalizovski, V. G. Galushko, A. V. Koloskov, and S. B. Kascheev, "Self-scattering effect of powerful HF radiation as observed in Europe and Antarctica", *RF Ionospheric Interactions Workshop*. Santa Fe, New Mexico, 17-20 April, 2005.
3. F. T. Djuth, P. A. Bernhardt, C. A. Tepley, J. A. Gardner, M. C. Kelley, A. L. Broadfoot, L. M. Kagan, M. P. Sulzer, J. H. Elder, C. Selcher, B. Isham, C. Brown, and H.C. Carlson, "Large Airglow Enhancements Produced via Wave-Plasma Interactions in Sporadic E", *Geophys. Res. Lett.*, vol. 26, pp. 1557-1560, 1999.
4. L. M. Kagan, M. C. Kelley, F. Garcia, P. A. Bernhardt, F. T. Djuth, M. P. Sulzer, C. A. Tepley, "The Structure of Electromagnetic Wave-Induced 557.7 nm Emission Associated with a Sporadic-E Event over Arecibo", *Phys. Rev. Lett.*, vol. 85, p. 218, 2000.
5. L. M. Kagan, N. V. Bakhmet'eva, V. V. Belikovich, A. V. Tolmacheva, and M. C. Kelley, "Structure and dynamics of sporadic E layers in the ionospheric E region", *Radio Sci.*, vol. 37, No. 6, p. 1106, 2002.
6. V. V. Belikovich, E. A. Benediktov, A. V. Tolmacheva, and N. V. Bakhmet'eva, *Ionospheric Research by Means of Artificial Periodic Irregularities*, Copernicus GmbH, Katlenburg-Lindau, Germany, 2002.
7. N. F. Blagoveshchenskaya, and O. A. Troshichev, "Ionospheric phenomena produced by modification experiments", *J. Atmos. Terr. Phys.*, vol. 58, pp. 397-406, 1996.
8. Y. M. Yampolski, V. S. Beley, S. B. Kascheev, A. V. Koloskov, V. G. Somov, D. L. Hysell, B. Isham, and M. C. Kelley, "Bistatic HF radar diagnostics of induced field-aligned irregularities", *J. Geophys. Res.*, vol. 102, No. A4, pp. 7461-7467, 1997.
9. P. V. Ponomarenko, A. V. Zalizovski, Yu. M. Yampolski, and D. L. Hysell, "Interaction between artificial ionospheric irregularities and natural MHD waves", *J. Geophys. Res.*, vol. 105, No. A1, pp. 171-181, 2000.
10. L. M. Kagan, M. J. Nicolls, M. C. Kelley, H. C. Carlson, V. V. Belikovich, N. V. Bakhmet'eva, G. P. Komrakov, T. S. Trondsen, and E. Donovan, "Observation of Radiowave-Induced Red Hydroxyl Emission at Low Altitude in the Ionosphere", *Phys. Rev. Lett.*, vol. 94, No. 9, p. 095004, 2005.
11. N. V. Bakhmet'eva, V. V. Belikovich, L. M. Kagan, A. A. Ponyatov, A. V. Tolmacheva, M. C. Kelley and M. J. Nicolls, "New results of the lower ionosphere studies by the method of resonant backscatter of radiowaves from artificial ionospheric irregularities", *Radiophys. Quantum Electron.*, vol. 48, No. 9, 2005.
12. Yu. M. Yampolski, "Echo-scattering of HF Signals on the Artificial Ionospheric Turbulence", *Radiophys. Quantum Elecron.*, vol. 32, No. 6, pp. 457-461, 1989.
13. Blagoveshchenskaya N. F., V. A. Bubnov, and V. A. Shelukhin, "Experimental studies of scattered HF diagnostic signals during ionospheric modification by powerful HF radio waves", *Radiophys. Quantum Electron.*, vol. 35, No. 1, pp. 24-30, 1992.
14. N. V. Bakhmet'eva, V. V. Belikovich, L. M. Kagan, and A. A. Ponyatov, "Sunset-to-sunrise characteristics of sporadic layers of ionization in the lower ionosphere observed by the method of resonance scattering of radio waves from artificial periodic inghomogeneities of the ionospheric plasma", *Radiophys. Quantum Electron.*, vol. 48, No. 1, pp. 14-28, 2005.
15. V. V. Belikovich, A. N. Karashtin, G. P. Komrakov, Yu. V. Shliugaev, "Simultaneous radiowave sounding of the midlatitude mesosphere at MF- and HF- frequency ranges", *Geomagnetism & Aeronomy*, vol. 43, No. 1, pp. 1-6, 2003.
16. V. L. Frolov, L. M. Kagan, G. P. Komrakov, E. N. Sergeev, E. A. Shorokhova, "Results of modification of the ionosphere sporadic-E layer by HF power radio emission", *Radiophys. Quantum Elecron.*, vol. 45, No. 12, pp. 917-928, 2002.
17. P. A. Bernhardt, W. A. Scales, S. M. Grach, A. N. Keroshtin, D. S. Kotik, S. V. Polyakov, "Excitation of artificial airglow by high power radio waves from the "SURA" ionospheric heating facility", *Geophys. Res. Lett.*, vol. 18, No. 8, pp. 1477-1480, doi: 10.1029/91GL01847, 1991.
18. P. A. Bernhardt, M. Wong, J. D. Huba, B. G. Fejer, L. S. Wagner, J. A. Goldstein, C. A. Selcher, V. L. Frolov, E. N. Sergeev, "Optical remote sensing of the thermosphere with HF pumped artificial airglow", *J. Geophys. Res.*, vol. 105, No. A5, pp. 10657-10672, doi: 10.1029/1999JA000366, 2000.
19. A. V. Gurevich, K. P. Zybin, H. C. Carlson, T. Pedersen, "Magnetic zenith effect in ionospheric modifications", *Phys. Lett. A*, vol. 305, No. 5. pp. 264-274, 2002.
20. A. V. Gurevich, K. P. Zybin, H. C. Carlson, "Magnetic Zenith Effect", *Radiophys. Quantum Electron.*, vol. 48, No. 9, 2005.
21. L. M. Kagan, "Aurora-associated phenomena and the e-POP mission", vol. 2, *Advances in Geosciences*, 2005.

22. G. P. Mantas and H. C. Carlson, "Reinterpretation of the 6300-E airglow enhancements observed in ionosphere heating experiments based on analysis of Platteville, Colorado, data". *J. Geophys. Res.*, vol. 101, No. A1, pp. 195-210, 1996.
23. T. B. Leyser, B. Thide, M. Waldenvik, E. Veszelei, V. L. Frolov, S. M. Grach, and G. P. Komrakov, "Downshifted maximum features in stimulated electromagnetic emission spectra", *J. Geophys. Res.*, vol. 99, No. A10, pp. 19555-19568, 1994.
24. T. B. Leyser, B. Thide, M. Waldenvik, S. Goodman, V. L. Frolov, S. M. Grach, A. N. Karashtin, G. P. Komrakov, and D. S. Kotik, "Spectral structure of stimulated electromagnetic emissions between electron cyclotron harmonic", *J. Geophys. Res.*, vol. 98, pp. 17597-17606, 1993.
25. T. B. Leyser, "Stimulated electromagnetic emissions by high frequency electromagnetic pumping of the ionospheric plasma", *Space Sci. Rev.*, vol. 98, pp. 223-328, 2001.
26. P. Stubbe, A. J. Stocker, F. Honary, T. R. Robinson, and T. B. Jones, "Stimulated electromagnetic emissions and anomalous HF wave absorption near electron gyroharmonics", *J. Geophys. Res*., vol. 99, No. A4, pp. 6233-6246, 1994.
27. V. L. Frolov, L. M. Erukhimov, L. M. Kagan, G. P. Komrakov, and E. N. Sergeev, "Two-component nature of the broad up-shifted maximum in stimulated electromagnetic emission spectra", *Phys. Rev. Lett*., vol. 81, pp. 1630-1633, 1998.
28. V. L. Frolov, E. N. Sergeev, E. N. Ermakova, G. P. Komrakov, and P. Stubbe, "Spectral features of stimulated electromagnetic emission measured in the $4.3 \div 9.5$ MHz pump wave frequency range", *Geophys. Res. Lett*., vol. 28, No. 16, pp. 3103-3106, 2001.
29. D. L. Hysell, M. C. Kelley, Y. M. Yampolski, V. S. Beley, A. V. Koloskov, P. V. Ponomarenko, and O. F. Tyrnov, "HF radar observations of decaying artificial field-aligned irregularities", *J. Geophys. Res.*, vol. 101, No. A12, pp. 26981-26993, 1996.
30. A. V. Koloskov, T. B. Leyser, Yu. M. Yampolski, and V. S. Beley, "HF pump-induced large scale radial drift of small scale magnetic field-aligned density striations", *J. Geophys. Res*., vol. 107, No. A7, doi: 10.1029/2001JA000154, 2002.
31. W. J. Peria and M. C. Kelley, "Convection electric field observations near the Arecibo HF heater beam", *J. Geophys. Res.*, vol. 106, No. A9, pp. 18517-18524, doi: 10.1029/2000JA000279, 2001.
32. P. V. Ponomarenko, T. B. Leyser, and B. Thide, "New electron gyroharmonic effects in HF scatter from pump-excited magnetic field-aligned ionospheric irregularities", *J. Geophys. Res*., vol. 104A, pp. 10081-10087, 1999.
33. F. Honary, T. R. Robinson, D. M. Wright, A. J. Stocker, M. T. Rietveld, and I. McCrea, "First direct observations of the reduced striations at pump frequencies close to the electron gyro harmonics", *Ann. Geophysicae*, vol. 17, pp. 1235-1238, 1999.
34. S. M. Grach, B. Thide, and T. B. Leyser, "Plasma waves near the double resonance layer in the ionosphere", *Radiophys. Quantum Electron.*, vol. 37, No. 5, pp. 617-633, 1994.
35. V. L. Frolov, L. M. Erukhimov, S. A. Metelev, and E. N. Sergeev, "Temporal behaviour of artificial small-scale ionospheric irregularities: Review of experimental results", *J. Atmos. Sol.-Terr. Phys.*, vol. 59, pp. 2317-2333, 1997.
36. L. J. Gelinas, M. C. Kelley, M. P. Sulzer, E. Mishin, M. J. Starks, "In situ observations during an HF heating experiment at Arecibo: Evidence for Z-mode and electron cyclotron harmonic effects", *J. Geophys. Res.*, vol. 108, No. A10, p. 1382, doi: 10.1029/2003JA009922, 2003.
37. T. D. Borisova, N. F. Blagoveshchenskaya, I. V. Moskvin, M. T. Rietveld, M. J. Kosch, and B. Thidé, "Doppler shift simulation of scattered HF signals during the Tromsø HF pumping experiment on 16 February, 1996", *Ann. Geophys*., vol. 20, pp. 1479-1486, 2002.
38. C. A. Gonzales, M. C. Kelley, L. A. Carpenter, and L. H. Holzworth, "Evidence for a magnetospheric effect on mid-latitude electric fields", *J. Geophys. Res.*, vol. 83, No. A9, pp. 4397-4399, 1978.
39. N. F. Blagoveshchenskaya, M. Yu. Chernyshev, and V. A. Kornienko, "Excitation of small-scale waves in the F region of the ionosphere by powerful HF radio waves", *J. Atmos. Terr. Phys.*, vol. 60, No. 12, pp. 1225-1232, 1998.
40. V. G. Sinitsin, M. C. Kelley, Yu. M. Yampolski, D. L. Hysell, A. V. Zalizovski, and P. V. Ponomarenko, "Ionospheric conductivities according to Doppler radar observations of stimulated turbulence", *J. Atmos. Terr. Phys*., vol. 61, No. 12, pp. 903-912, 1999.
41. N. F. Blagoveshchenskaya, T. D. Borisova, V. A. Kornienko, T. B. Leyser, M. T. Rietveld, and B. Thidé, "Artificial field-aligned irregularities in the nightside auroral ionosphere", *Adv. Space Res.*, 2005. (In press).
42. M. C. Kelley, T. L. Arce, J. Salowey, M. Sulzer, T. Armstrong, M. Carter, and L. Duncan, "Density depletion at the ten meter scale induced by Arecibo heater", *J. Geophys. Res.*, vol. 100, No. 5, p. 17367, 1995.
43. T. L. Franz, M. C. Kelley, and A. V. Gurevich, "Radar backscattering from artificial field-aligned irregularities", *Radio Sci.*, vol. 34, No. 2, pp. 465-476, 1999.

44. N. F. Blagoveshchenskaya, T. D. Borisova, V. A. Kornienko, M. T. Rietveld, L. M. Kagan, Y. M. Yampolsky, V. L. Frolov, V. G. Galushko, A. V. Koloskov, S. B. Kascheev, A. V. Zalizovky, G. V. Vertogradov, and M. C. Kelley, "Probing of medium-scale traveling ionospheric disturbances using HF-induced scatter targets", *Ann. Geophys*, 2005 (submitted).
45. V. L. Frolov, D. I. Nedzvedski, Yu. M. Yampolski, A. V. Kolockov, A. V. Zalizovski, V. L. Galushko, S. B. Kascheev, G. G. Vertogradov, V. G. Vertogradov, N. F. Blagoveschenskaya, V. A. Kornienko, L. M. Kagan, M. C. Kelley, "Spectral characteristics of signals scattered by artificial small-scale irregularities for the pump frequency close to a frequency of electron gyro harmonics", *in Proc. of XX1 Russian National conference on Radiowave Propagation*, Ioshkarala, Russia, 2005 (in Russian).

Оптическая и радиочастотная диагностика ионосферы над нагревным стендом Сура. Обзор результатов

Л. М. Каган, М. Дж. Николлс, М. К. Келли, В. Л. Фролов, В. В. Беликович, Н. В. Бахметьева, Г. П. Комраков, Д. И. Недзветский, В. П. Урядов, Ю. М. Ямпольский, В. Г. Галушко, А. В. Колосков, А. В. Зализовский, С. Б. Кащеев, Н. Ф. Благовещенская, В. А. Корниенко, Т. Д. Борисова, А. В. Гуревич, Г. Г. Вертоградов, В. Г. Вертоградов, Т. С. Трондсен, Е. Донован

Рассматривается схема и результаты оптической и радиочастотной диагностики ионосферы методом обратного рассеяния во время нагревной кампании 10-20 августа, 2004 г. Нагрев осуществлялся при помощи стенда Сура, расположенного вблизи Нижнего Новгорода, Россия. В этой кампании оптические измерения впервые сопровождались диагностикой плазмы методом искусственных периодических неоднородностей, а также многопунктовыми измерениями обратнорассеянных сигналов, что является примером использования кластеризации инструментов для улучшения результатов исследований. Результаты, которые уже опубликованы в Radiophysics and Quantum Electronics и Physical Review Letters в данной работе только подытожены. Новые результаты включают в себя: смещение оптической эмиссии на $1 \div 2°$ от магнитного зенита, уширение спектров обратнорассеянных сигналов при нагреве на частоте вблизи четвертой гармоники гирочастоты электронов, наблюдение саморассеянных сигналов на второй гармонике частоты нагрева, первые наблюдения вектора скорости дрейфа плазмы и электрического поля, при помощи вытянутых вдоль поля неоднородности, проверка возможности влияния рефракционного механизма на допплеровское смещения частоты саморассеянных сигналов и первые наблюдения синхронных вариаций саморассеянных и обратнорассеянных сигналов. Наблюдения электрического поля подтвердили предположение о том, что процессы в высоких широтах могут воздействовать на ионосферу в средних широтах над такими установками, как Сура.

Оптична та радіочастотна діагностика іоносфери над нагрівним стендом Сура. Огляд результатів

Л. М. Каган, М. Дж. Ніколлс, М. К. Келлі, В. Л. Фролов, В. В. Белікович, Н. В. Бахмет'єва, Г. П. Комраков, Д. І. Недзветський, В. П. Урядов, Ю. М. Ямпольський, В. Г. Галушко, О. В. Колосков, А. В. Залізовський, С. Б. Кащеєв, Н. Ф. Благовещенська, В. А. Корнієнко, Т. Д. Борисова, О. В. Гуревич, Г. Г. Вертоградов, В. Г. Вертоградов, Т. С. Трондсен, Е. Донован

Розглядається схема та результати оптичної та радіочастотної діагностики іоносфери методом зворотного розсіяння під час нагрівної кампанії 10-20 серпня 2004 р. Нагрівання здійснювалося за допомогою стенда Сура, розташованого поблизу Нижньо-

го Новгорода, Росія. У цій кампанії оптичні виміри вперше супроводжувалися діагностикою плазми методом штучних періодичних неоднорідностей, а також багатопунктовими вимірами зворотнорозсіяних сигналів, що є прикладом використання кластеризації приладів для поліпшення результатів досліджень. Результати, які вже опубліковані в Radiophysics and Quantum Electronics та Physical Review Letters, у даній роботі лише підсумовані. Нові результати включають: зсув оптичної емісії на $1 \div 2°$ від магнітного зеніту, розширення спектрів зворотнорозсіяних сигналів при нагріванні на частоті поблизу четвертої гармоніки гірочастоти електронів, спостереження саморозсіяних сигналів на другій гармоніці частоти нагрівання, перші спостереження вектора швидкості дрейфу плазми і електричного поля за допомогою витягнутих уздовж поля неоднорідностей, перевірка можливості впливу рефракційного механізму на доплерівський зсув частоти саморозсіяних сигналів і перші спостереження синхронних варіацій саморозсіяних та зворотнорозсіяних сигналів. Спостереження електричного поля підтвердили припущення про те, що процеси у високих широтах можуть впливати на іоносферу в середніх широтах над такими установками, як Сура.